Very-High (Cm scale) Resolution Multichannel Seismology

J. F. Gettrust[*], W. T. Wood[*], M. M. Rowe[*], J. G. Kosalos[**], and S. Szender[**]

[*]Naval research laboratory
Code 7432
Stennis Space Center, MS 39529
Email: gettrust@nrlssc.navy.mil

[**]Alliant Techsystems
Marine Systems West
6500 Harbour Heights Pkwy
Mukilteo, WA 98275

Abstract

Seismic imaging techniques together with some non-linear beamforming are used to resolve objects and structures in the shallow subsurface (to ~3 m depth) using 15-35 kHz band signals. The instrument used for this study is proportioned after conventional multichannel seismic systems, but is about 3 orders of magnitude smaller. This geometry and very-high frequency source allows us to image structures on a scale of ~0.1 m, and to detect even smaller-scale objects. While imaging theory is independent of scale, practical application of high-frequency imaging requires continued improvement in our ability to dynamically locate the spatial position of both source and receivers.

Introduction

The theory used for seismic imaging of the earth's subsurface [1] is independent of scale. Therefore, small scale (<1m) acoustic anomalies theoretically may be imaged with the small-scale equivalent of a conventional multichannel seismic system. In shallow-water environments these anomalies may be related to natural geologic activity, (small vents or faults) or to indigenous biologic activity, (mounds, boroughs, or large shells), or even to human activity (shipwrecks, plane wrecks, explosive mines, waste mounds, etc.). Imaging of surface and subsurface impedance mismatches with sub-meter resolution allows detection and more accurate determination of the nature of small anomalies. The multiple offset data obtained with multichannel seismic (MCS) systems makes it possible to measure the compressional and shear velocities within the sediments. These data make it possible to estimates the physical properties of the sediments and, therefore, provide a critical constraint to interpretation of the seismic imagery.

Instrumentation and Data

The data (acoustic targets) used for this study were located in a test range in Puget Sound. The targets were 0.025m diameter armored coaxial cables, some positioned on and some beneath the seafloor. The system used to take these data is scaled directly from the Deep Towed Acoustics/Geophysics System (DTAGS) that was developed at the Naval research laboratory (NRL) several years ago [2]. DTAGS has been used successfully to study subbottom structures on the scale of ~4 m; the new system was designed to resolve features ~0.1 m scale. The 16 receivers used with the very-high frequency system are 0.2 m apart and are attached to the same rigid frame as the source (Figure 1). The nearest offset hydrophone is 3.441 m from the source while the furthest offset sensor is 6.441 m from the source. The source has a 40° beam width and is directed back toward the array at an angle of 30° from vertical. The receiving hydrophones have omni-directional response within the lower halfspace. Each shot trace (i.e., the data recorded by an individual hydrophone for a given source pulse) in this survey consists of 10000 samples with a sample interval of 1.0 x10-5 s. For each survey line, the source was fired 100 times, once every 0.2 s; the shot spacing ranged from 0.06 m to 0.09 m making the lines 6 to 9 m in length. The effective penetration in the soft sediments sampled was up to ~10 m. Data were acquired using both single frequency (25 kHz) tone bursts of 4 cycles with wider frequency-band FM sweeps. Figure 2 shows the amplitude spectra of signals from the two lines discussed in this study. Each spectra computed from an average of 1500 independent "shots".

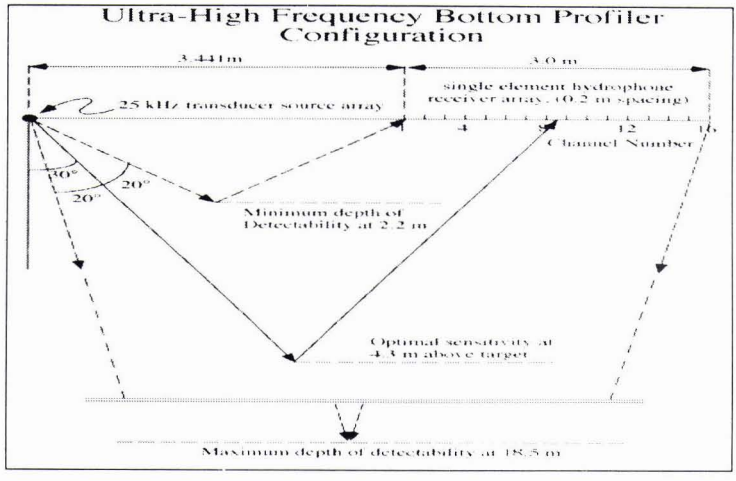

Figure 1. Geometry of UHF-MCS system. Note the directionality of the source.

Note the significant increase in bandwidth for the chirp data (see Figure 2) allowing for significantly enhanced time resolution. The spectral chirp data were deconvolved using an estimate of the wavelet made by stacking, in phase, all water bottom arrivals on channel 2 (the nearest-offset channel) of that line. Note that there was no facility on the MCS system to obtain the source function directly so we used the direct water bottom reflection. Here we assume that the uppermost subbottom structure is laterally uncorrelated and will interfere destructively, whereas the directly reflected source signature will add constructively.

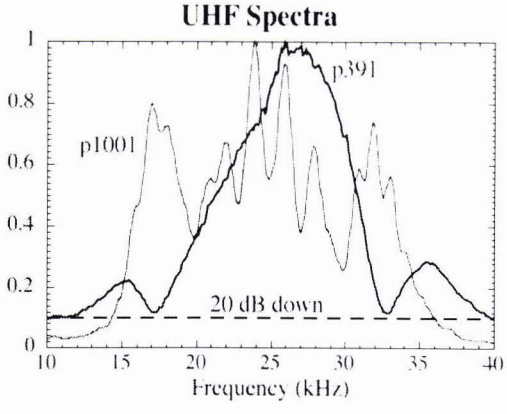

Figure 2. Amplitude spectra of 4-cycle pulse (dark line) and 15-35 kHz chirp (light line) source signals

Practical Aspects of Imaging

The objective of this study was to use seismic imaging theory and methods adapted from conventional hydrocarbon exploration which, usually, makes use of signals in the 10-80 Hz band, to image small scale acoustic anomalies on and just below the sea floor. Previously, we have used these techniques to study features to ~4 m scale to more than 750 m depth using a multichannel seismic system with a 250 Hz - 650 Hz source. Our experience with that system indicated that although the imaging theory is certainly independent of scale, practical aspects of positioning, (towing) the system, and therefore significant portions of the processing are not [3]. These aspects become even more critical when using the very-high frequency (UHF) signals in the 10-40 kHz band where wavelengths are on the order of centimeters.

In particular, uncertainties from GPS positioning of several m are of virtually no consequence for conventional exploration seismic wavelengths of 20 m, but for wavelengths of 0.06 m uncertainties of this magnitude substantially

degrade the ability to correlate events from different survey lines. Fortunately, uncertainties in relative position (shot to shot spacing) can be constrained to be much smaller. Although steady towing at speeds less than 1 kt is extremely difficult, low sea state, careful operation, and the relatively short time over which the experiment is performed allow for a reasonably consistent (~0.005 m) shot spacing over the course of a short, 8 m survey line. To further constrain shot spacing system accelerations in the vertical and the two horizontal planes also were recorded. The integrals of the these accelerations provide significant improvement in determination of relative shot spacing and shot-receiver depths. As we will show, further engineering efforts in terms of system stability will be required to reach the full potential of the resolution available with a 10-40 kHz source frequency.

In contrast to these inter-shot limitations, some aspects of this scale of exploration are significantly simpler than in conventional MCS work. For example, because the source and receivers are mounted on a rigid frame, the uncertainty in the relative positions of the source and receivers is essentially zero. There is no streamer feathering (i.e., curvature of the receive array), and no problems with portions of the streamer sinking or floating, (changes in the orientation, or pitch are small relative to the resolution of the system). Also, because of the frequencies used, one need not be concerned with maintaining a quarter wavelength source depth to reduce ghosting. In fact the system is towed at depth to maintain good angular coverage over the target. Multiples and ghosts from the air water interface tend to be significantly scattered due to the roughness of this interface at the scale of ~0.01 m, and generally arrive too late to interfere with subsurface reflections.

Another fortuitous aspect of processing these UHF data is the relatively small variation in compressional velocity both vertically and laterally in the sediments penetrated. As P-wave velocity increases, penetration is reduced, so the velocity in the penetrated sediments ranges from 1474 m/s in the water column to rarely more than ~1550 m/s, or a change of ~5%. Contrast this with the more than 100% change for conventional seismic work. As shown later these relatively mild velocity changes greatly simplify the velocity analyses and migrations, two important and usually time consuming parts of conventional imaging.

In light of the above observations the first priority in imaging these data was to determine the actual shot spacing for each line. This can be accomplished in several ways, one of which is to iteratively migrate the near trace gather with the known water velocity and trial shot spacings. The water velocity was determined to be 1474 ± 3 m/sec, calculated from the slope of the direct-wave arrival across the array. Preliminary velocity analyses confirmed this value and also confirmed that the receiver array was flying level (with respect to the resolution of the system). Proper shot spacings were determined by varying shot separations used for migration until the diffraction hyperbolae from rough water bottom features or in one case a buoy floating 2 m above the bottom (see Figure 3) were optimally collapsed. In some cases the optimal collapse was not quite complete due to slight changes in shot spacing over the course of the line. The shot spacing corresponding to optimal near-trace migration was determined to be reasonably consistent within a line (± 0.005 m), but varied among lines between 0.06 and 0.1 m. Another way to determine shot spacing is to identify the same small bottom feature on both the near and far channel records. Half of the distance between the two channels divided by the number of shots between the features' appearance on the two records yields another estimate of the shot spacing. These two methods yielded consistent estimates. Because the shot spacing remained reasonably constant over the lines used here, and because irregular shot spacing complicates the processing, the acceleration values were not used and the shot spacing was assumed to be constant.

Imaging the Data Field

The primary goal of imaging is the notion of focusing; this is done by applying operators that concentrate the scattered wave energy back to a reflection "point". Although in some cases a traditional imaging approach of common midpoint gathering followed by move out correction, stacking, migration may produce a satisfactory image with UHF data, we wish to address the problem more comprehensively.

When used as an imaging tool, beamforming is equivalent to prestack migration. Consider an image point $P(x_i,z_i)$ located in the vertical plane defined by our linear array. This point will be ensonified by several shots as the system passes by. When each source pulse arrives we assume based on Huygens' principal that this image point behaves as a secondary point source. The spherical wave (we assume for now a constant velocity medium) emanating from this secondary source strikes each receiver located at (x_r,z_r) in the array at a time given by:

$$t(x_r, z_r) = \frac{\left[(x_s - x_i)^2 + (z_s - z_i)\right]^{1/2}}{V} + \frac{\left[(x_r - x_i)^2 + (z_r - z_i)^2\right]^{1/2}}{V} \qquad (1)$$

where V is the velocity of the medium, and (x_s,z_s) is the source location. The first term is simply the time to the secondary source, and the second term is the time from the secondary source to the receiver. Summing along this trajectory (linearly interpolating as necessary for digitized data) is the mathematical equivalent of physically bending the array in a circular arc whose center is occupied by the point P. This summation is performed for each image point $P(x_i,z_i)$ in the vertical plane to produce the final image. Sample amplitudes are multiplied by their arrival time to compensate for spherical divergence.

Beamforming, or migrating in this ray-based manner also allows for a simple way of incorporating the directivity of the source. Recall that the source transducer used in this study is directed 30° from the vertical, and has a beam width of 40°, (suggested by the asymmetric nature of the large diffraction hyperbola in Figure 3, top, left). For the ray from the source to each image point (first term of Equation 1) the angle with the vertical is easily computed. Gain is applied to the sample amplitudes along the trajectory corresponding to this image point to compensate for the source directivity. When the image point is too far outside the beam (where source levels fall below the noise level) it cannot be imaged so no trajectory is computed and the image value is set to zero.

This operation was applied to every shot of line p1001 (Figure 3 top, left) with the result shown in Figure 3 center, left. As with any prestack migration the diffraction from the buoy is neatly collapsed, while the very flat, somewhat dipping seafloor is not significantly altered. Careful inspection directly below the buoy reveals the cable, which has apparently sunk several cm into the mud.

Note the difference in frequency content between Figures 3 top, left and center left. The beamforming was applied as described above to one shot at a time. The contributions to the image space from neighboring shots will overlap and because of the uncertainties in the shot position the image contributions from these separate shots may interfere destructively, when we would like them to interfere constructively. One way to mitigate this problem is to slightly blur the images by reduce the effective frequency range through computing the instantaneous amplitude and bandpass filtering. This reduces the frequency range from 15-35 kHz to 1-15 kHz, making the uncertainties in shot position smaller relative to the dominant wavelength, and aiding constructive interference. Resolution and polarity information are sacrificed to obtain a clearer image.

Beamforming with Robust Norms

The nature of the beamforming algorithm allows for the easy implementation of a more sophisticated measure of coherency along the trajectory of Equation 1 than a simple summation. Some of the data presented in Figure 3 were computed using a family of norms which are computed using the generalized mean [4] which is defined by:

$$L_j^{\alpha} = \left(\sum_{i=1}^{n} \mathrm{sgn}(x_{j,i}) \left| x_{j,i} \right|^{\alpha} \right)^{1/\alpha} \qquad (2)$$

where the function sgn() (the sign of the variable) is required to maintain the integrity of the polarity information, i.e. on which side of the origin the norm lies. It has been shown [5] that for small signal-to-noise ratios with mixed-Gaussian noise distributions, $0.33 < \alpha < 0.5$ produces a significantly better estimate of the signal than does the conventional summation ($\alpha = 1$). Note that when $\alpha = 0$, the generalized mean is equivalent to "hard limiting", a technique that works well when the noise field is uniformly distributed (reference).

We incorporated the L^{α} norm operator into the beamformer by accumulating at each image point the term under the radical in Equation 2 regardless of which shot the samples came from. After all shots had contributed to the image the a root and rest of Equation 2 was computed. The algorithm was then applied to line p1001 with the results shown in Figure 3, (bottom, left). Note the significant enhancement of the signal compared to Figure 3 (center, left), although the cable near the water bottom is still difficult to distinguish from the water bottom reflection.

Because one important application of this kind of processing is the detection of small objects often we may wish to emphasize point diffractors, and de-emphasize layered geology, essentially the opposite of conventional imaging strategy. One way to accomplish this is to use the apparent dip of diffraction hyperbolas to discriminate against layered horizons. Horizontal events are easily removed from unmigrated common offset gathers by frequency-wavenumber, (F-K) filtering (Yilmaz 1988). Channel 2 of line P1001 before F-K filtering, (Figure 3 top, left) is dominated by the water bottom event. After F-K filtering to remove horizontal events, (Figure 3 top, right) the diffraction hyperbolas from the cable and the attached buoy are quite evident. The F-K filtering is applied to each common offset gather independently.

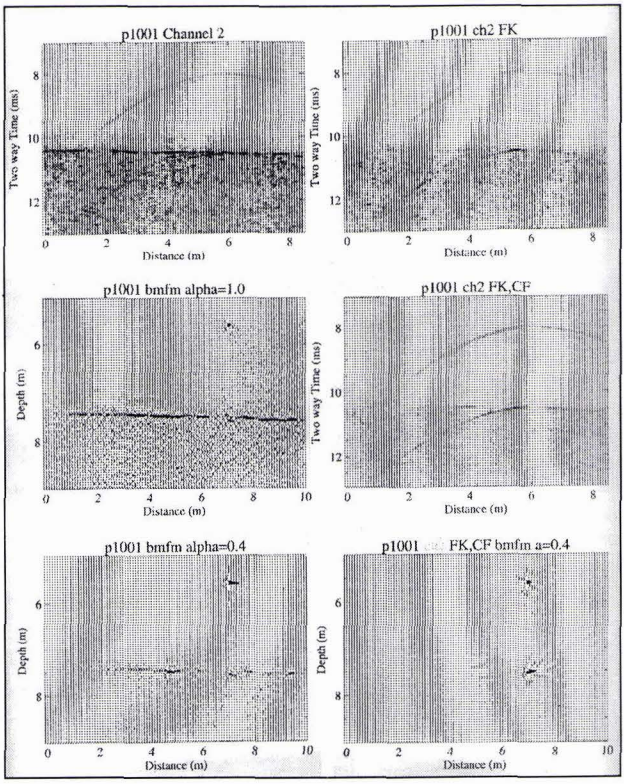

Figure 3.

We incorporated the L^{α} norm operator into the beamformer by accumulating at each image point the term under the radical in Equation 2 regardless of which shot the samples came from. After all shots had contributed to the image the α root and rest of Equation 2 was computed. The algorithm was then applied to line p1001 with the results shown in Figure 3, (bottom, left). Note the significant enhancement of the signal compared to Figure 3 (center, left), although the cable near the water bottom is still difficult to distinguish from the water bottom reflection.

Because one important application of this kind of processing is the detection of these small objects we may wish to emphasize point diffractors, and de-emphasize layered geology, essentially the opposite of conventional imaging strategy. One way to accomplish this is to use the apparent dip of diffraction hyperbolas to discriminate against layered horizons. Horizontal events are easily removed from unmigrated common offset gathers by frequency-wavenumber, (F-K) filtering [6]. Channel 2 of line P1001 before F-K filtering, (Figure 3 top, left) is dominated by the water bottom event. After F-K filtering to remove horizontal events, (Figure 3 top, right) the diffraction hyperbolas from the cable and the attached buoy are quite evident. The F-K filtering is applied to each common offset gather independently.

To further enhance these coherent events a coherency filter can be applied. Much of the noise in these data is incoherent from trace to trace within a shot gather or from shot to shot in a common offset gather. At each sample of each trace in the common offset gather semblance is measured over a suite of trajectories within user specified dips. In these examples this range was -6 to +8 samples per trace and each trajectory extended 3 traces on either side of the current trace. A time window of 10 samples was used for the semblance calculation. Semblance values range from 0 for completely uncorrelated events to 1 for identical events along the specified trajectory. The semblance value from the most coherent direction was multiplied to the original amplitude of the sample. The same procedure is applied to each sample of the common offset gather, resulting in a significant reduction in the incoherent noise (Figure 3 center, right). In this Figure the point diffractors dominate the image.

Once the F-K and coherency filters were applied to each common offset gather the data were reordered into shot gathers and the beamforming algorithm was applied as before, again with a=0.4, (Figure 3 bottom, right). Note the spectacular enhancement of the point diffractors, particularly the cable near the surface which was previously barely detectable. Both the buoy and the cable can be easily located to within ~0.1 m.

Geophysical Parameters

The multiple offset data taken with MCS systems allows one to obtain estimates of the compressional velocities within the sediments. This is done by inverting the reflection hyperbola for a given shot (common shot point or CSP) or at a given point (common mid point of CMP). This technique works very well even though reflection times do not actually hyperbola for multi-layer case [1]. Compressional velocity estimates for data taken with the ultra-high frequency MCS system are presented in Figure 4. These data suggest that there is significant lateral variability in the uppermost sediment column although the absolute change in velocities is ~5%, much smaller than we encounter with deeper probing systems.

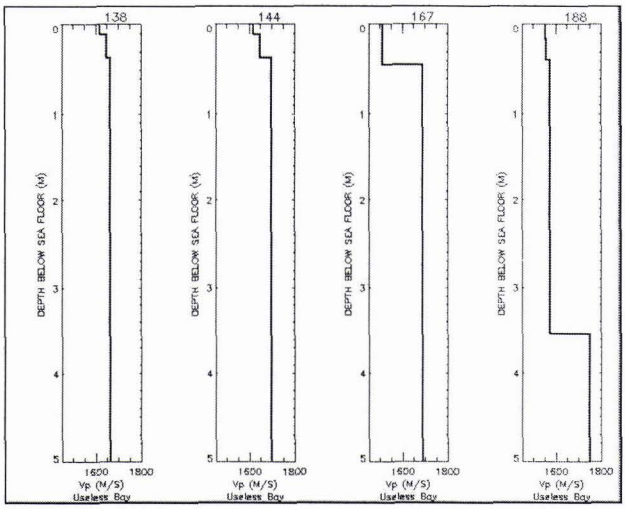

Figure 4.

Another advantage of the multiple-offset data is that it is possible to place constraints on shear velocities in the sediments. This can be done using amplitude versus offset (AVO) analysis [7] or spectrum versus offset (SVO) [8]. Both techniques were tried with these data, but to resolve the low shear velocities associated with these sediments requires a greater range of wavenumbers than is available with these data.

Conclusions

Modern digital seismic data processing techniques can be successfully applied to ultra-high frequency data (10's of kHz) when certain caveats are observed. Objects as small as 2.5 cm dia. were located to within ~0.1 m relative to the system, and bathymetric features on the order of several cm were clearly imaged. This is despite the fact that the data were "blurred" somewhat by uncertainties in shot spacing. The data generally require rather sophisticated prestack imaging (migration or equivalently beamforming) which is capable of incorporating strong source directivity. The use of robust estimators used in concert with the imaging algorithm provide significantly improved results.

Relatively small variations in P-wave velocity, very precise knowledge of the receiver array relative to the source, and lack of surface multiples make these data generally easier to process (image) than conventional (10-80 Hz) data. To fully exploit the potential of ultra-high frequency MCS, improvements in the absolute positioning of the system and the relative shot to shot positioning are required. However, even with current limitations on positioning, our data show that significant improvements in sediment classification (physical properties) and identification of small objects on or beneath the seafloor can be had using MCS technology.

Acknowledgements

The authors thank Alliant Techsystems for permission to publish the data. This work was supported by the Office of Naval Research Program Element/Project Number 0602435N/BE-35-2-02. This paper is NRL Conribution #A/7432--96-0022.

References

[1] J. F. Clearbout, Fundamentals of geophysical data processing with applications to petroleum prospecting. New York, McGraw Hill, 1976

[2] J. F. Gettrust, J. H. Ross, and M. M. Rowe, Development of a low frequency, deep tow geoacoustics System, Sea Technology, 199

[3] M. M. Rowe and J. F. Gettrust, Fine structure of methane hydrate-bearing sediments on the Blake Outer Ridge as determined from deep-tow multichannel seismic data, Journ. Geophys. Res., vol. 98 pp. 463-473, 1993

[4] Abramowitz and Stegun, Handbook of mathematical functions with formulas, graphs, and mathematical tables, Washington D. C., U. S. Dept. of Commerce National Bureau of Standards, 1964.

[5] J. F. Gettrust, Ph.D. dissertation, Univ. of Wisconsin-Madison, 1973

[6] O. Yilmaz, Seismic data processing, Society of Exploration Geophysicists, Investigations in Geophysics Vol. 2, 1988.

[7] J. Castagna and M. Backus, Offset-dependent reflectivity - theory and practice of AVO analysis, Society of Exploration Geophysicists, Investigations in Geophysics Vo:. 8, 1993.

[8] J. F. Gettrust and M. M. Rowe, Constraints on shear velocities in deep-ocean sediments as determined from deep-tow multichannel seismic data, in Shear Waves in Marine Sediments, Kluwer Academic publishers, pp. 369-378, 1991.